

# Pulse-width-induced polarization enhancement of optically pumped N-V electron spin in diamond

YUMENG SONG,<sup>1,†</sup> YU TIAN,<sup>2,†</sup> ZHIYI HU,<sup>1</sup> FEIFEI ZHOU,<sup>1</sup> TENG TENG XING,<sup>1</sup> DAWEI LU,<sup>2</sup> BING CHEN,<sup>1,6</sup> YA WANG,<sup>3,4,5</sup> NANYANG XU,<sup>1,7</sup> AND JIANGFENG DU<sup>3,4,5,8</sup>

<sup>1</sup>School of Electronic Science and Applied Physics, Hefei University of Technology, Hefei 230009, China

<sup>2</sup>Shenzhen Institute for Quantum Science and Engineering and Department of Physics, Southern University of Science and Technology, Shenzhen 518055, China

<sup>3</sup>Hefei National Laboratory for Physical Sciences at the Microscale and Department of Modern Physics, University of Science and Technology of China, Hefei 230026, China

<sup>4</sup>CAS Key Laboratory of Microscale Magnetic Resonance, University of Science and Technology of China, Hefei 230026, China

<sup>5</sup>Synergetic Innovation Center of Quantum Information and Quantum Physics, University of Science and Technology of China, Hefei 230026, China

<sup>6</sup>e-mail: bingchenphysics@hfut.edu.cn

<sup>7</sup>e-mail: nyxu@hfut.edu.cn

<sup>8</sup>e-mail: djf@ustc.edu.cn

Received 8 January 2020; revised 2 June 2020; accepted 3 June 2020; posted 4 June 2020 (Doc. ID 386983); published 14 July 2020

The nitrogen-vacancy (N-V) center in diamond is a widely used platform for quantum information processing and sensing. The electron-spin state of the N-V center could be initialized, read out optically, and manipulated by resonate microwave fields. In this work, we analyze the dependence of electron-spin initialization on widths of laser pulses. We build a numerical model to simulate this process and to verify the simulation results in experiments. Both simulations and experiments reveal that shorter laser pulses are helpful to the electron-spin polarization. We therefore propose to use extremely short laser pulses for electron-spin initialization. In this new scheme, the spin-state contrast could be improved about 10% in experiments by using laser pulses as short as 4 ns in width. Furthermore, we provide a mechanism to explain this effect, which is due to the occupation time in the meta-stable spin-singlet states of the N-V center. Our new scheme is applicable in a broad range of N-V-based applications in the future. © 2020 Chinese Laser Press

<https://doi.org/10.1364/PRJ.386983>

## 1. INTRODUCTION

The N-V center in diamond is a widely used physical platform for quantum information science and technology due to its good controllability and long coherence at room temperature [1–5]. The electron spin, together with nearby nuclear spins, works as a quantum register for quantum computation [2,6–12] or a nanoscale probe for sensing magnetic fields [13–27], electric fields [28], and temperatures [29–31]. This also enables further applications of the N-V center in nanoscale nuclear magnetic resonance (NMR) [18,32–34] and electron spin resonance (ESR) [35,36]. A fundamental requirement of these applications is that the spin state of the N-V center can be initialized and read out easily, which is traditionally realized through the same optical pumping process due to a spin-dependent intersystem crossing (ISC) mechanism.

The energy levels of the N-V center are shown in Fig. 1(b). When pumped with a laser pulse, the electron spin is excited from the ground spin-triplet ( ${}^3A_2$ ) states to the excited states ( ${}^3E$ ) [37–43]. After a few nanoseconds, the electron spin decays back to the ground state and emits a fluorescence photon.

Alternatively, an ISC may happen via metastable spin-singlet states ( ${}^1E$  and  ${}^1A$ ) with no fluorescence photon emitted, where the probability from  $m_s = \pm 1$  to  $m_s = 0$  is much larger than that of the reverse process [26,44–46]. This induces a spin-dependent fluorescence photon count to be detected; hence, the spin-state of the N-V center can be read out in experiment. After repeating the process a few times, the electron spin is prepared in the ground  $m_s = 0$  with a high probability [47]. The mechanism of ISC has been studied and attributed to spin-orbital and electron-phonon interactions [43]. Recently, a microscopic model is also provided to explain the electronic states of the N-V center, the optical transitions, and the ISC [48].

As a fundamental technique for initialization and readout, the optical pumping process has been parametrically studied, and the transition rates between the electron-spin states have been measured experimentally [43,48,49]. In a typical N-V experiment at room temperature, the spin polarization of the N-V center to  $m_s = 0$  is estimated to be 90% [50], and a fluorescence contrast between the  $m_s = 0$  and  $m_s = \pm 1$  to be over 20% can be observed when driving the electron spin

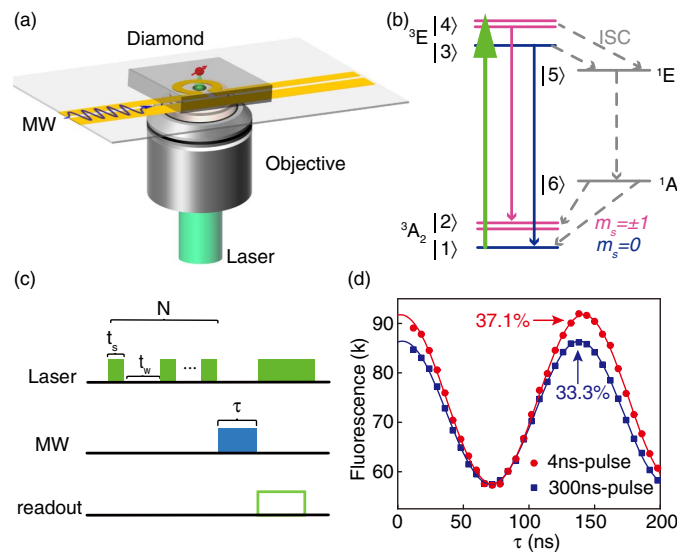


**Fig. 1.** Experimental scheme and main result. (a) Experimental setup and a single N-V center in diamond. (b) Electron-spin energy-level of N-V center and the spin dynamics of the pumping process at room temperature. The transition of pumping laser (532 nm) is indicated by the green solid line, while the radiative (nonradiative) transition is the red solid (gray dashed) line. (c) Pulse sequence of the electron-spin Rabi oscillation using repeatedly pulse-width-modulated laser. (d) Effect of pulse-width modulation in electron-spin Rabi oscillation. Blue (red) points are experimental data with 300 ns (4 ns) laser pulses with the pulse sequence shown in (c). The number 33.3% (37.1%) noted in the plot is the contrast value between the  $m_s = 0$  and  $m_s = -1$  spin states using the corresponding scheme. Each data point is obtained from  $10^{10}$  Rabi sequence repetitions for signal accumulation.

with a resonant microwave field (i.e., via Rabi experiment). Furthermore, several new approaches have been proposed to improve the optical readout efficiency of spin states; further, the effect of the pumping laser on the nuclear-spin polarization is also studied in experiments [51–57].

In this paper, we study the effect of the pumping laser's width on the electron-spin polarization and provide a more efficient optical initialization scheme in experiments. We change the experimental pumping sequence by repeatedly applying short laser pulses instead of a single long pulse until a steady spin-state is achieved. Numerical simulation indicates better polarization could be achieved when the pulse width decreases. This result is then verified by observing the spin-state contrast of Rabi oscillation in experiments. We show that the mechanism of this effect is the overall dwelling time of the N-V center in the meta-stable spin-singlet states. Consequently, by reducing the pulse width to 4 ns, we observe a 10% enhancement in spin-state contrast. The signal-to-noise ratio (SNR) for quantum sensing experiment scales as the square root of total measurement time [47,58]. To realize the same SNR, our method only spends  $0.9^2$  of the time with the traditional laser pulse method. It implies an improvement at nearly 20% in terms of experimental efficiency. In addition, we evaluate the influences from other experimental parameters, including the laser power, microwave power, and the wait time between laser pulses. This work provides new insights and improvement of efficiency for the optical polarizing process in N-V experiments and is thus useful in future applications.

## 2. RESULTS

The essential idea of this work is to examine the dependence of the spin-state polarization on laser pulse widths in the pumping

process. The traditional pulse sequence for laser polarization consists of a single square laser pulse followed with a wait time. In this work, we extend this single-loop mode to a more generalized mode, as shown in Fig. 1(c), i.e., a multiloop sequence by repeatedly applying laser pulses with a wait time in between for  $N$  times. For each case,  $N$  is large enough to saturate the polarization.

In order to evaluate the efficiency of this new sequence, a rate equation model is built to simulate the pumping process and calculate the expected polarization at the end of the process. Details of the numerical model and simulation parameters are discussed in the following sections. We apply this new sequence in experiments and parametrically study the performance of the process. Direct detection of the electron-spin polarization requires either single-shot spin readout at a cryogenic temperature [5] or the help of an ancillary nuclear spin [59]. In this work, we use the spin-state contrast to evaluate the electron-spin polarization instead, which is more generalized at ambient conditions. The contrast is defined as  $(I_{\max} - I_{\min})/I_{\max}$ , where  $I_{\max}$  and  $I_{\min}$  are the maximal and minimal fluorescence counts fitted from the detected signal in a Rabi experiment, respectively. The pulse sequence is shown in Fig. 1(c). After polarizing the electron spin, a resonant microwave is applied to drive the spin to oscillate between  $m_s = 0$  and  $m_s = \pm 1$  states. Since the spin-state  $m_s = 0$  ( $\pm 1$ ) is associated with a higher (lower) detected fluorescence counts, the contrast is actually linear with the polarization in experiments.

We first examine the pumping process by using different widths of laser pulses in the above sequence. By repeating the pulse loops, we observe the polarization directly in numerical simulations. In Fig. 2(a), the results show that, for sequences with shorter laser pulses, the polarization improves more slowly

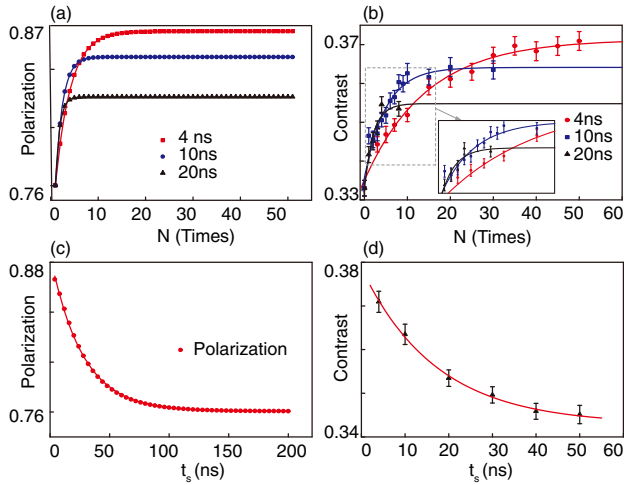


**Fig. 2.** Numerical simulations and their corresponding experimental results. (a) For laser pulses with three different widths, the highest polarization that can be achieved in simulation is dependent on the repeating times  $N$ . (b) The measured contrast using different pulse widths and repetitions in Rabi experiment. (c) There is a continuous decrease of the highest polarization when the pulse width  $t_s$  is increasing from 4 to 200 ns in simulation. (d) Measured polarization (contrast) for pulse widths from 4 to 50 ns. Each experimental point is obtained from  $10^{10}$  Rabi sequence [Fig. 1(c)] repetitions for signal accumulation.

but finally achieves a higher level and vice versa. To verify these trends, we perform the corresponding experiments using the same pulse sequence. For each pulse width, we increase the loop number  $N$  and measure the Rabi oscillation signals. The fitted contrast, which matches well with the simulation results, is shown in Fig. 2(b). Both results show that shorter laser pulses are more efficient in the laser pumping process for initialization of the electron spin.

Further, we study the saturated polarization level for each pulse width  $t_s$ , i.e., the stable value when  $N$  is large enough. The simulation result is shown in Fig. 2(c), where an exponentially decaying polarization is observed as the pulse width  $t_s$  increases. This simulation matches well with the above individual observations. We also verify this numerical expectation with experiments. For each  $t_s$ , we increase the repetition times  $N$  and wait time  $t_w$  until the spin-state contrast saturates. The final contrast for each  $t_s$  in Fig. 2(d) matches well with the numerical simulations. Based on these results, we reveal the relation between polarization and pulse width  $t_s$ .

In experiments, we demonstrate that this new pumping method with repeatedly applied short laser pulses indeed enhances polarization in the N-V center. For comparison, we measure the Rabi signals using 300 ns (a typical width in traditional experiments) and 4 ns laser pulses by this new method, as shown in Fig. 1(d), respectively. The experimental result presents a nearly 10% enhancement in spin-state contrast using this new approach compared with the traditional pumping method. Since the readout stage and the detection noise remain unchanged, this improvement implies a nearly 20% savings of time cost to achieve the same SNR in experiments.

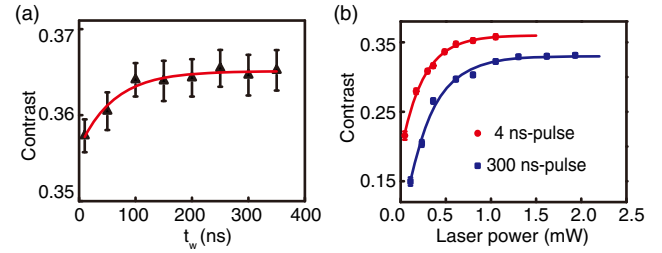


**Fig. 3.** Measured Rabi oscillation in terms of spin contrast for (a) different wait time  $t_w$  and (b) different laser powers. Each data point is obtained from  $10^{10}$  Rabi sequence [Fig. 1(c)] repetitions for signal accumulation.

To show the robustness of our method, we also investigate the influence of different wait time  $t_w$  and laser power in experiments. In Fig. 3(a), the wait time  $t_w$  is swept from 10 to 350 ns and the contrast is measured accordingly, where we set  $t_s = 4$  ns and  $N = 30$ . The experimental result shows that, for  $t_w$  greater than 100 ns, the polarization efficiency remains almost stable. For the laser powers, we test both the standard single-loop (the 300 ns pulse) and the multiloops schemes (the 4 ns pulse) in Fig. 3(b). In both cases, the polarization performance is proportional to the laser power and saturates when the power is over 1 mW. Hence, it can be concluded that, for either the traditional scheme or our scheme, the effect of the laser power is almost irrelevant in boosting the polarization performance, except for a slight discrepancy between the 4 and 300 ns curves. This is mainly attributed to the low efficiency of the acousto-optic modulator (AOM) working in the short-pulse regime.

### 3. NUMERICAL SIMULATIONS

Here, we describe the details of the numerical simulation. The dynamics of the laser pumping process is shown in Fig. 1(b). The ground (excited) state is a spin triplet  $^3A_2$  ( $^3E$ ) with energy splitting  $D_{gs} = 2.87$  GHz ( $D_{es} = 1.41$  GHz) between  $m_s = 0$  and  $m_s = \pm 1$  states at zero magnetic field. Because the dynamics in  $m_s = +1$  and  $-1$  are equivalent in the pumping process, we use a reduced six-level system without loss of generality, including the ground states ( $|1\rangle$ ,  $|2\rangle$ ), excited states ( $|3\rangle$ ,  $|4\rangle$ ), and the spin-singlet system involved in ISC ( $|5\rangle$ ,  $|6\rangle$ ). We employ a rate equation model to simulate the transition process. Here, the state of the N-V center is represented in a vector  $\mathbf{P} = (P_1, P_2, P_3, P_4, P_5, P_6)$  with  $P_i$  the population on state  $|i\rangle$  and  $\sum_i P_i = 1$ . The population vector changes during the pumping process according to equations, which can be expressed in the matrix form as

$$\frac{d}{dt}\mathbf{P} = M_i\mathbf{P}, \quad (1)$$

where  $M_0$  ( $M_1$ ) denotes the transition matrix when laser illumination is on (off). The matrix element of  $M_0$  ( $M_1$ ) is defined from the transition speed  $k_{ij}$  from state  $|i\rangle$  to  $|j\rangle$  as

**Table 1. Transition Rates in Numerical Simulation**

$k_{ij}$	Transition Rate (ns <sup>-1</sup> )	$k_{ij}$	Transition Rate (ns <sup>-1</sup> )
$k_{13}, k_{24}$	0.628	$k_{45}$	0.1884
$k_{31}, k_{42}$	0.4396	$k_{56}$	6.28
$k_{35}$	0.0314	$k_{61}$	0.020724
$k_{62}$	0.013816	$k_{6*}$	$k_{61} + k_{62}$
$k_{3*}$	$k_{31} + k_{35}$	$k_{4*}$	$k_{42} + k_{45}$

$$M_0 = \begin{bmatrix} -k_{13} & 0 & k_{31} & 0 & 0 & k_{61} \\ 0 & -k_{24} & 0 & k_{42} & 0 & k_{62} \\ k_{13} & 0 & -k_{3*} & 0 & 0 & 0 \\ 0 & k_{24} & 0 & -k_{4*} & 0 & 0 \\ 0 & 0 & k_{35} & k_{45} & -k_{56} & 0 \\ 0 & 0 & 0 & 0 & k_{56} & -k_{6*} \end{bmatrix} \quad (2)$$

and

$$M_1 = \begin{bmatrix} 0 & 0 & k_{31} & 0 & 0 & k_{61} \\ 0 & 0 & 0 & k_{42} & 0 & k_{62} \\ 0 & 0 & -k_{3*} & 0 & 0 & 0 \\ 0 & 0 & 0 & -k_{4*} & 0 & 0 \\ 0 & 0 & k_{35} & k_{45} & -k_{56} & 0 \\ 0 & 0 & 0 & 0 & k_{56} & -k_{6*} \end{bmatrix}. \quad (3)$$

Further, details of  $k_{ij}$  in simulation are shown in Table 1, which are extracted from Refs. [38,39,43].

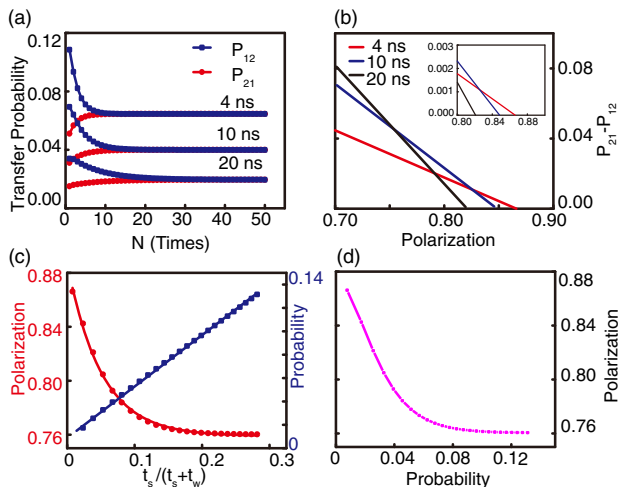


**Fig. 4.** Mechanism and simulation results. (a) The population transfer  $P_{21}$  and  $P_{12}$  eventually converge to the same value as the repetition  $N$  increases. Here,  $P_{ij}$  denotes the population transfer from  $|i\rangle$  to  $|j\rangle$ . (b) Difference between  $P_{21}$  and  $P_{12}$ , which indicates the net transfer between  $|1\rangle$  and  $|2\rangle$ . (c) Probability (blue) at meta-stable spin-singlet states ( $|5\rangle$  and  $|6\rangle$ ) and the corresponding final polarization (red) with the occupation of the laser over all the process  $t_s/(t_s + t_w)$ . (d) Direct relation between the final polarization and the probability at meta-stable spin-singlet states.

The pumping process in a typical N-V experiment consists of a single square laser pulse and a wait time, as shown in Fig. 1(c). The target of this process is to initialize the electronic spin into the  $m_s = 0$  ground state with high probability. Here, in order to analyze the pulse-width-induced effect on spin polarization, we replace the traditional single square laser pulse with  $N$  repeatedly applied short pulses, i.e., the setting in our scheme. As shown in Fig. 1(d), each short pulse is of width  $t_s$  and a wait time  $t_w$  is inserted in between. We simulate this process using the above equation and calculate the polarization at the end of this process. In simulations with fixed parameters  $t_s$  and  $t_w$ , the polarization is approaching a stable level when the repeating times  $N$  increases as in Fig. 4(a). Thus, to get the best polarization for each  $t_s$  or  $t_w$ , we choose  $N$  to be large enough (e.g., 400 for most of the cases).

#### 4. MECHANISM

Here, we consider the case where the pumping process starts with a thermal state  $P = (\frac{1}{3}, \frac{2}{3}, 0, 0, 0, 0)$ . For a single-pulse loop with a short laser pulse and a wait time, the increased polarization depends on the value  $P_{21} - P_{12} > 0$ , where  $P_{ij}$  denotes the transferred population from state  $|i\rangle$  to  $|j\rangle$  in a single loop. As the pulse loop starts to repeat, the population  $P_2$  increases while  $P_1$  decreases; thus,  $P_{21}$  goes smaller and  $P_{12}$  goes bigger. Finally, a steady state is obtained with  $P_{12} = P_{21}$ , and the pumping process is completed. This process is shown in Fig. 4(a), where for different  $t_s$ , the value  $P_{21}$  ( $P_{12}$ ) changes with different speeds. This difference induces different final polarization of the steady states. We also show this effect by plotting the net transferred population  $P_{21} - P_{12}$  in a single loop toward the polarization in Fig. 4(b). For each pulse width  $t_s$ , the best polarization is achieved in the steady state where  $P_{21} - P_{12} = 0$ . From this simulation, we see that smaller  $t_s$  is associated with better polarization, which matches well with experimental results.

The reason for this pulse-width-induced polarization difference, however, is the overall population of the N-V center in the spin-singlet meta-stable states, i.e., states  $|5\rangle$  and  $|6\rangle$ . During the initialization process, the transferred population from state  $|3\rangle$  ( $|4\rangle$ ) to  $|5\rangle$  increases (decreases) until a steady state is reached. Once the N-V center is on the state  $|5\rangle$ , it falls down to state  $|6\rangle$  immediately and, subsequently, onto the ground state  $|1\rangle$  or  $|2\rangle$ . Since the transition rates from state  $|6\rangle$  to states  $|1\rangle$  and  $|2\rangle$  are almost the same, this transition transfers similar amounts of population to the ground spin-states and reduces the final polarization of the whole pumping process.

Therefore, reducing the dwelling time on the meta-stable states would increase the final polarization level in the process. To confirm, we integrate the population and calculate the probability of the N-V center on states  $|5\rangle$  and  $|6\rangle$  during the pumping process (including the wait time) in simulation. The relation between the probability at the meta-stable states and the occupation of the laser over all the process  $t_s/(t_s + t_w)$  is shown in Fig. 4(c), where the probability decreases almost linearly with the occupation value. A direct relation between the final polarization and the meta-stable state probability is also shown in Fig. 4(d). These results can be used to explain

the mechanism of the pulse-width-induced polarization enhancement, which is in fact due to the reduction of the dwelling time on the meta-stable spin-singlet states during the pumping process.

## 5. EXPERIMENTS

To demonstrate, we use a home-built optically detected magnetic resonance (ODMR) system to address and manipulate the single N-V-based centers in a type-IIa, single-crystal synthetic diamond sample (Element Six). As shown in Fig. 1(a), the 532 nm pumping laser is focused on the sample via a 100× oil-immersed objective. The emitted fluorescence ranging from 650 to 800 nm is spatially filtered through a 50 μm pinhole and finally collected by an avalanche photodiode (APD) for single-photon counting. A low magnetic field with a few Gauss is applied along the N-V axis to split the energy levels of  $m_s = \pm 1$ . A microwave field used to drive the electron-spin state is generated from the microwave source (Rohde & Schwartz SMIQ03) and amplified by a wideband amplifier (Mini-Circuits ZHL-42W) to drive the transition between  $m_s = 0$  and  $m_s = -1$ . An impedance-matched copper slot line with a gap of 0.1 mm with an  $\Omega$ -type ring (inner diameter 300 μm) mounted on a coverslip is used to hold the sample and radiate the microwave fields.

In this work, the pumping laser beam is modulated by a 350 MHz AOM before being applied on the sample. The AOM is driven by a 2.6 GS/s AWG (Tektronix AWG610) with an output bandwidth over 800 MHz, which is capable of generating laser pulses as short as 4 ns. In order to suppress the laser leakage, another AOM is used following the first one, which turns off the laser in the rest time of the experiments. In order to measure the spin-state contrast, we perform a Rabi oscillation experiment, as shown in Fig. 1(c), where the initialization with traditional square (repeatedly shorter) laser pulses is applied on the N-V center followed with a resonant variable-width microwave pulse and another laser pulse for state readout. The signal is fitted with a cosine function, and the contrast is calculated with the fitting parameters.

## 6. DISCUSSION AND CONCLUSION

Considering the total overhead in experiments, our method requires an extra time cost of a few microseconds to perform the laser pulse and wait time for many repetitions. In most N-V applications, such as sensing remote spins or magnetic signals, the experiment operation time ranges from hundreds of microseconds to hundreds of milliseconds [35,60]. This increase in initialization overhead (<1%) is minor compared with the enhanced performance in experimental efficiency. For the effect of N-V optical ionization, the steady-state charge-state efficiency, which is caused by both the ionization (N-V<sup>-</sup> to N-V<sup>0</sup>) and recombination (N-V<sup>0</sup> to N-V<sup>-</sup>) process, depends on the illumination intensity and wavelength together at regular laser powers [58,61]. In our experiment, the laser wavelength (532 nm) remains unchanged, and the power is fixed in most of the cases. To further consider the effect of the laser's pulse width in the ionization process, a more complicated experiment setup should be used, where a 594 nm laser is applied to a single-shot readout of the charge states [52].

To conclude, we analyze the pulse-width-induced effect on the electron-spin polarization of the N-V center in the optical initialization process and provide a new scheme to polarize the electron spin with repeatedly applied short laser pulses. This new scheme provides an enhancement of about 10% in readout efficiency, leading to a nearly 20% saving of time cost in experiments. Moreover, we build a numerical model to simulate the optical initialization process and calculate the dependence of the polarization using different parameters. The result matches well with the experimental observations of the spin-state contrast. By analyzing the mechanism of our new scheme, we conclude that the superiority of our method is mainly due to the reduction of the dwelling time on the meta-stable spin-singlet states during the initialization process. Our new scheme could be applied to N-V-based quantum applications in a broad range and may shed light on understanding the optical initialization process in the N-V centers.

**Funding.** National Key Research and Development Program of China (2017YFA0305000, 2018YFA0306600, 2019YFA0308100); Fundamental Research Funds for the Central Universities (PA2019GDQT0023); National Natural Science Foundation of China (11604069, 11761131011, 11775209, 11875159); CAS (GJJSTD20170001, QYZDY-SSW-SLH004); Anhui Initiative in Quantum Information Technologies (AHY050000); Innovative Program of Development Foundation of Hefei Center for Physical Science and Technology (2017FXCX005).

**Disclosures.** The authors declare no conflicts of interest related to this paper.

<sup>†</sup>These authors contributed equally to this work.

## REFERENCES

1. P. C. Maurer, G. Kucsko, C. Latta, L. Jiang, N. Y. Yao, S. D. Bennett, F. Pastawski, D. Hunger, N. Chisholm, M. Markham, D. J. Twitchen, J. I. Cirac, and M. D. Lukin, "Room-temperature quantum bit memory exceeding one second," *Science* **336**, 1283–1286 (2012).
2. L. Childress, M. V. Gurudev Dutt, J. M. Taylor, A. S. Zibrov, F. Jelezko, J. Wrachtrup, P. R. Hemmer, and M. D. Lukin, "Coherent dynamics of coupled electron and nuclear spin qubits in diamond," *Science* **314**, 281–285 (2006).
3. T. D. Ladd, F. Jelezko, R. Laflamme, Y. Nakamura, C. Monroe, and J. L. O'Brien, "Quantum computers," *Nature* **464**, 45–53 (2010).
4. G.-Q. Liu and X.-Y. Pan, "Quantum information processing with nitrogen-vacancy centers in diamond," *Chin. Phys. B* **27**, 020304 (2018).
5. L. Robledo, L. Childress, H. Bernien, B. Hensen, P. F. A. Alkemade, and R. Hanson, "High-fidelity projective read-out of a solid-state spin quantum register," *Nature* **477**, 574–578 (2011).
6. M. V. G. Dutt, L. Childress, L. Jiang, E. Togan, J. Maze, F. Jelezko, A. S. Zibrov, P. R. Hemmer, and M. D. Lukin, "Quantum register based on individual electronic and nuclear spin qubits in diamond," *Science* **316**, 1312–1316 (2007).
7. P. Neumann, N. Mizuochi, F. Rempp, P. Hemmer, H. Watanabe, S. Yamasaki, V. Jacques, T. Gaebel, F. Jelezko, and J. Wrachtrup, "Multiparticle entanglement among single spins in diamond," *Science* **320**, 1326–1329 (2008).
8. G. Waldherr, Y. Wang, S. Zaiser, M. Jamali, T. Schulte-Herbrüggen, H. Abe, T. Ohshima, J. Isoya, J. F. Du, P. Neumann, and J. Wrachtrup, "Quantum error correction in a solid-state hybrid spin register," *Nature* **506**, 204–207 (2014).

9. T. H. Taminiau, J. Cramer, T. van der Sar, V. V. Dobrovitski, and R. Hanson, "Universal control and error correction in multi-qubit spin registers in diamond," *Nat. Nanotechnol.* **9**, 171–176 (2014).
10. T. H. Taminiau, J. J. T. Wagenaar, T. van der Sar, F. Jelezko, V. V. Dobrovitski, and R. Hanson, "Detection and control of individual nuclear spins using a weakly coupled electron spin," *Phys. Rev. Lett.* **109**, 137602 (2012).
11. F. Kong, C. Ju, Y. Liu, C. Lei, M. Wang, X. Kong, P. Wang, P. Huang, Z. Li, F. Shi, L. Jiang, and J. Du, "Direct measurement of topological numbers with spins in diamond," *Phys. Rev. Lett.* **117**, 060503 (2016).
12. K. Xu, T. Xie, Z. Li, X. Xu, M. Wang, X. Ye, F. Kong, J. Geng, C. Duan, F. Shi, and J. Du, "Experimental adiabatic quantum factorization under ambient conditions based on a solid-state single spin system," *Phys. Rev. Lett.* **118**, 130504 (2017).
13. S. Zaiser, T. Rendler, I. Jakobi, T. Wolf, S.-Y. Lee, S. Wagner, V. Bergholm, T. Schulte-Herbrüggen, P. Neumann, and J. Wrachtrup, "Enhancing quantum sensing sensitivity by a quantum memory," *Nat. Commun.* **7**, 12279 (2016).
14. I. Jakobi, P. Neumann, Y. Wang, D. B. R. Dasari, F. El Hallak, M. A. Bashir, M. Markham, A. Edmonds, D. Twitchen, and J. Wrachtrup, "Measuring broadband magnetic fields on the nanoscale using a hybrid quantum register," *Nat. Nanotechnol.* **12**, 67–72 (2017).
15. T. Uden, P. Balasubramanian, D. Louzon, Y. Vinkler, M. B. Plenio, M. Markham, D. Twitchen, A. Stacey, I. Lovchinsky, A. O. Sushkov, M. D. Lukin, A. Retzker, B. Naydenov, L. P. McGuinness, and F. Jelezko, "Quantum metrology enhanced by repetitive quantum error correction," *Phys. Rev. Lett.* **116**, 230502 (2016).
16. M. Pfender, N. Aslam, H. Sumiya, S. Onoda, P. Neumann, J. Isoya, C. A. Meriles, and J. Wrachtrup, "Nonvolatile nuclear spin memory enables sensor-unlimited nanoscale spectroscopy of small spin clusters," *Nat. Commun.* **8**, 834 (2017).
17. T. Roskopf, J. Zopes, J. M. Boss, and C. L. Degen, "A quantum spectrum analyzer enhanced by a nuclear spin memory," *NPJ Quantum Inf.* **3**, 33 (2017).
18. N. Aslam, M. Pfender, P. Neumann, R. Reuter, A. Zappe, F. F. de Oliveira, A. Denisenko, H. Sumiya, S. Onoda, J. Isoya, and J. Wrachtrup, "Nanoscale nuclear magnetic resonance with chemical resolution," *Science* **357**, 67–71 (2017).
19. C. H. Li, Y. Dong, J. Y. Xu, D. F. Li, X. D. Chen, A. M. Du, Y. S. Ge, G. C. Guo, and F. W. Sun, "Enhancing the sensitivity of a single electron spin sensor by multi-frequency control," *Appl. Phys. Lett.* **113**, 072401 (2018).
20. C. L. Degen, "Scanning magnetic field microscope with a diamond single-spin sensor," *Appl. Phys. Lett.* **92**, 243111 (2008).
21. P. Maletinsky, S. Hong, M. S. Grinolds, B. Hausmann, M. D. Lukin, R. L. Walsworth, M. Loncar, and A. Yacoby, "A robust scanning diamond sensor for nanoscale imaging with single nitrogen-vacancy centres," *Nat. Nanotechnol.* **7**, 320–324 (2012).
22. L. Rondin, J. P. Tetienne, T. Hingant, J. F. Roch, P. Maletinsky, and V. Jacques, "Magnetometry with nitrogen-vacancy defects in diamond," *Rep. Prog. Phys.* **77**, 056503 (2014).
23. M. S. Grinolds, S. Hong, P. Maletinsky, L. Luan, M. D. Lukin, R. L. Walsworth, and A. Yacoby, "Nanoscale magnetic imaging of a single electron spin under ambient conditions," *Nat. Phys.* **9**, 215–219 (2013).
24. G. Balasubramanian, I. Y. Chan, R. Kolesov, M. Al-Hmoud, J. Tisler, C. Shin, C. Kim, A. Wojcik, P. R. Hemmer, A. Krueger, T. Hanke, A. Leitenstorfer, R. Bratschitsch, F. Jelezko, and J. Wrachtrup, "Nanoscale imaging magnetometry with diamond spins under ambient conditions," *Nature* **455**, 648–651 (2008).
25. P. F. Wang, C. Y. Ju, F. Z. Shi, and J. F. Du, "Optimizing ultrasensitive single electron magnetometer based on nitrogen-vacancy center in diamond," *Chin. Sci. Bull.* **58**, 2920–2923 (2013).
26. A. Gruber, A. Dräbenstedt, C. Tietz, L. Fleury, J. Wrachtrup, and C. von Borczyskowski, "Scanning confocal optical microscopy and magnetic resonance on single defect centers," *Science* **276**, 2012–2014 (1997).
27. J. R. Maze, P. L. Stanwix, J. S. Hodges, S. Hong, J. M. Taylor, P. Cappellaro, L. Jiang, M. V. Dutt, E. Togan, A. S. Zibrov, A. Yacoby, R. L. Walsworth, and M. D. Lukin, "Nanoscale magnetic sensing with an individual electronic spin in diamond," *Nature* **455**, 644–647 (2008).
28. F. Dolde, H. Fedder, M. W. Doherty, T. Nöbauer, F. Rempp, G. Balasubramanian, T. Wolf, F. Reinhard, L. C. L. Hollenberg, F. Jelezko, and J. Wrachtrup, "Electric-field sensing using single diamond spins," *Nat. Phys.* **7**, 459–463 (2011).
29. P. Neumann, I. Jakobi, F. Dolde, C. Burk, R. Reuter, G. Waldherr, J. Honert, T. Wolf, A. Brunner, and J. H. Shim, "High-precision nanoscale temperature sensing using single defects in diamond," *Nano Lett.* **13**, 2738–2742 (2013).
30. G. Kucsko, P. C. Maurer, N. Y. Yao, M. Kubo, H. J. Noh, P. K. Lo, H. Park, and M. D. Lukin, "Nanometre-scale thermometry in a living cell," *Nature* **500**, 54–58 (2013).
31. D. M. Toyli, C. F. de las Casas, D. J. Christle, V. V. Dobrovitski, and D. D. Awschalom, "Fluorescence thermometry enhanced by the quantum coherence of single spins in diamond," *Proc. Natl. Acad. Sci. USA* **110**, 8417–8421 (2013).
32. T. Staudacher, F. Shi, S. Pezzagna, J. Meijer, J. Du, C. A. Meriles, F. Reinhard, and J. Wrachtrup, "Nuclear magnetic resonance spectroscopy on a (5-nanometer)<sup>3</sup> sample volume," *Science* **339**, 561–563 (2013).
33. H. J. Mamin, M. Kim, M. H. Sherwood, C. T. Rettner, K. Ohno, D. D. Awschalom, and D. Rugar, "Nanoscale nuclear magnetic resonance with a nitrogen-vacancy spin sensor," *Science* **339**, 557–560 (2013).
34. I. Lovchinsky, A. O. Sushkov, E. Urbach, N. P. de Leon, S. Choi, K. De Greve, R. Evans, R. Gertner, E. Bersin, C. Müller, L. McGuinness, F. Jelezko, R. L. Walsworth, H. Park, and M. D. Lukin, "Nuclear magnetic resonance detection and spectroscopy of single proteins using quantum logic," *Science* **351**, 836–841 (2016).
35. F. Shi, Q. Zhang, P. Wang, H. Sun, J. Wang, X. Rong, M. Chen, C. Ju, F. Reinhard, H. Chen, J. Wrachtrup, J. Wang, and J. Du, "Single-protein spin resonance spectroscopy under ambient conditions," *Science* **347**, 1135–1138 (2015).
36. E. Bourgeois, A. Jarmola, P. Siyushev, M. Gulka, J. Hruby, F. Jelezko, D. Budker, and M. Nesladek, "Photoelectric detection of electron spin resonance of nitrogen-vacancy centres in diamond," *Nat. Commun.* **6**, 8577 (2015).
37. V. M. Acosta, A. Jarmola, E. Bauch, and D. Budker, "Optical properties of the nitrogen-vacancy singlet levels in diamond," *Phys. Rev. B* **82**, 201202 (2010).
38. T. Chakraborty, J. Zhang, and D. Suter, "Polarizing the electronic and nuclear spin of the NV-center in diamond in arbitrary magnetic fields: analysis of the optical pumping process," *New J. Phys.* **19**, 073030 (2017).
39. L. Robledo, H. Bernien, T. Van Der Sar, and R. Hanson, "Spin dynamics in the optical cycle of single nitrogen-vacancy centres in diamond," *New J. Phys.* **13**, 025013 (2011).
40. W. Happer, "Optical pumping," *Rev. Mod. Phys.* **44**, 169–249 (1972).
41. V. Jacques, P. Neumann, J. Beck, M. Markham, D. Twitchen, J. Meijer, F. Kaiser, G. Balasubramanian, F. Jelezko, and J. Wrachtrup, "Dynamic polarization of single nuclear spins by optical pumping of nitrogen-vacancy color centers in diamond at room temperature," *Phys. Rev. Lett.* **102**, 057403 (2009).
42. A. Leneff and S. C. Rand, "Electronic structure of the N-V center in diamond: theory," *Phys. Rev. B* **53**, 13441–13455 (1996).
43. N. B. Manson, J. P. Harrison, and M. J. Sellars, "Nitrogen-vacancy center in diamond: model of the electronic structure and associated dynamics," *Phys. Rev. B* **74**, 104303 (2006).
44. T. Gaebel, M. Domhan, I. Popa, C. Wittmann, P. Neumann, F. Jelezko, J. R. Rabeau, N. Stavrias, A. D. Greentree, S. Praver, J. Meijer, J. Twamley, P. R. Hemmer, and J. Wrachtrup, "Room-temperature coherent coupling of single spins in diamond," *Nat. Phys.* **2**, 408–413 (2006).
45. R. Hanson, F. M. Mendoza, R. J. Epstein, and D. D. Awschalom, "Polarization and readout of coupled single spins in diamond," *Phys. Rev. Lett.* **97**, 087601 (2006).
46. J. Harrison, M. J. Sellars, and N. B. Manson, "Measurement of the optically induced spin polarisation of N-V centres in diamond," *Diam. Relat. Mater.* **15**, 586–588 (2006).
47. C. L. Degen, F. Reinhard, and P. Cappellaro, "Quantum sensing," *Rev. Mod. Phys.* **89**, 035002 (2017).
48. M. L. Goldman, M. W. Doherty, A. Sipahigil, N. Y. Yao, S. D. Bennett, N. B. Manson, A. Kubanek, and M. D. Lukin, "State-selective

- intersystem crossing in nitrogen-vacancy centers," *Phys. Rev. B* **91**, 165201 (2015).
49. M. L. Goldman, A. Sipahigil, M. W. Doherty, N. Y. Yao, S. D. Bennett, M. Markham, D. J. Twitchen, N. B. Manson, A. Kubanek, and M. D. Lukin, "Phonon-induced population dynamics and intersystem crossing in nitrogen-vacancy centers," *Phys. Rev. Lett.* **114**, 145502 (2015).
  50. T. van der Sar, Z. H. Wang, M. S. Blok, H. Bernien, T. H. Taminiau, D. M. Toyli, D. A. Lidar, D. D. Awschalom, R. Hanson, and V. V. Dobrovitski, "Decoherence-protected quantum gates for a hybrid solid-state spin register," *Nature* **484**, 82–86 (2012).
  51. M. Steiner, P. Neumann, J. Beck, F. Jelezko, and J. Wrachtrup, "Universal enhancement of the optical readout fidelity of single electron spins at nitrogen-vacancy centers in diamond," *Phys. Rev. B* **81**, 035205 (2010).
  52. B. J. Shields, Q. P. Unterreithmeier, N. P. de Leon, H. Park, and M. D. Lukin, "Efficient readout of a single spin state in diamond via spin-to-charge conversion," *Phys. Rev. Lett.* **114**, 136402 (2015).
  53. D. A. Hopper, R. R. Grote, A. L. Exarhos, and L. C. Bassett, "Near-infrared-assisted charge control and spin readout of the nitrogen-vacancy center in diamond," *Phys. Rev. B* **94**, 241201 (2016).
  54. F. M. Hrubesch, G. Braunbeck, M. Stutzmann, F. Reinhard, and M. S. Brandt, "Efficient electrical spin readout of NV<sup>-</sup> centers in diamond," *Phys. Rev. Lett.* **118**, 037601 (2017).
  55. L. Jiang, J. S. Hodges, J. R. Maze, P. Maurer, J. M. Taylor, D. G. Cory, P. R. Hemmer, R. L. Walsworth, A. Yacoby, and A. S. Zibrov, "Repetitive readout of a single electronic spin via quantum logic with nuclear spin ancillae," *Science* **326**, 267–272 (2009).
  56. S. A. Wolf, I. Rosenberg, R. Rapaport, and N. Bar-Gill, "Purcell-enhanced optical spin readout of nitrogen-vacancy centers in diamond," *Phys. Rev. B* **92**, 235410 (2015).
  57. N. Xu, Y. Tian, B. Chen, J. Geng, X. He, Y. Wang, and J. Du, "Dynamically polarizing spin register of N-V centers in diamond using chopped laser pulses," *Phys. Rev. Appl.* **12**, 024055 (2019).
  58. J. F. Barry, J. M. Schloss, E. Bauch, M. J. Turner, C. A. Hart, L. M. Pham, and R. L. Walsworth, "Sensitivity optimization for NV-diamond magnetometry," *Rev. Mod. Phys.* **92**, 015004 (2020).
  59. X. Rong, J. Geng, F. Shi, Y. Liu, K. Xu, W. Ma, F. Kong, Z. Jiang, Y. Wu, and J. Du, "Experimental fault-tolerant universal quantum gates with solid-state spins under ambient conditions," *Nat. Commun.* **6**, 8748 (2015).
  60. N. Bar-Gill, L. M. Pham, A. Jarmola, D. Budker, and R. L. Walsworth, "Solid-state electronic spin coherence time approaching one second," *Nat. Commun.* **4**, 1743 (2013).
  61. N. Aslam, G. Waldherr, P. Neumann, F. Jelezko, and J. Wrachtrup, "Photo-induced ionization dynamics of the nitrogen vacancy defect in diamond investigated by single-shot charge state detection," *New J. Phys.* **15**, 013064 (2013).